ISBN: 978-3-95450-253-0 ISSN: 2673-5571 doi:10.18429/JACoW-HB2023-TUC4I1

A KICKER IMPEDANCE REDUCTION SCHEME WITH DIODE STACK AND RESISTOR AT THE RCS IN J-PARC

Y. Shobuda, H. Harada, P.K. Saha, T. Takayanagi, F. Tamura, T. Togashi, Y. Watanabe, K. Yamamoto, M. Yamamoto, JAEA, Tokaimura, Ibaraki, Japan

Abstract

At the 3-GeV Rapid Cycling Synchrotron (RCS) within the Japan Proton Accelerator Research Complex (J-PARC), kicker impedance causes beam instability. A 1 MW-beam with a large emittance can be delivered to the Material and Life Science Experimental Facility (MLF) by suppressing beam instabilities without the need for a transverse feedback system simply by turning off the sextuple magnets. However, we require other high-intensity and high-quality beams with smaller emittances for the Main Ring (MR). To address this, we proposed a scheme for suppressing the kicker impedance using a diode stack and resistors, which effectively reduces beam instability. Importantly, these devices have a negligible effect on the extracted beam from the RCS.

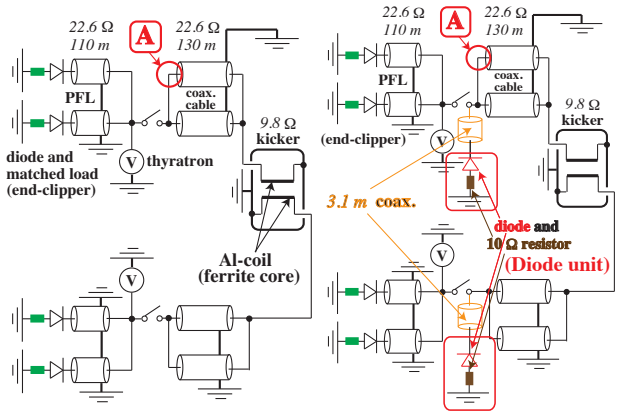

Figure 1: Kicker without (left) and with diode units (right).

INTRODUCTION

The RCS in J-PARC [1] has accelerated two bunches, each containing 4.15×10^{13} particles, from 400 MeV to 3 GeV in 20 ms. This acceleration, with a repetition rate of 25 Hz, has made 1 MW-beam operation possible [2].

The RCS provides proton beams downstream to both the MLF and the MR [3]. The standard unnormalized transverse painting emittance, the unnormalized value of the entire painting area, for the MLF, is relatively large (e.g., 200π mm.mrad), which can easily stabilize a high-intensity beam (even a 1 MW-beam). However, the emittance must be less than 50π mm.mrad for the MR, because the beams extracted from the RCS are delivered to the MR through the beam extraction line with a small mechanical aperture, exciting a large residual dose.

Since the RCS was designed such that all impedance sources are below the impedance budget, except the kicker impedance, the beam instability [4] excited by the extraction kicker magnet has been the main issue that limits the generation of the high-intensity beam [5].

However, theoretical, simulation, and experimental measurements have clarified the mechanism of space-charge effects, including indirect space-charge effects, to suppress beam instability in a space-charge-dominated machine (like the RCS) [6–8]. Hence, if the machine parameters, including tunes, chromaticities,... are appropriately chosen, the 1 MW-beam is realized without any transverse feedback system for a larger emittance beam by making use of the indirect space charge effects.

On the other hand, small emittance broadens the transverse tune spreads due to space-charge effects, restricting the variable tune-tracking pattern during the acceleration period. Furthermore, suppression of beam instability is more difficult with a smaller transverse emittance than with a larger emittance, because the suppression effect due to the indirect space charge force is relatively mitigated for the smaller transverse emittance beam [7, 8].

In the end, lowering the kicker impedance [4] is required for the generation of high-intensity and high-quality small emittance beams by the RCS.

As shown in Fig. 1, the kicker at the RCS is a transmission line-type embedding two ferrite cores [9]. The kicker has four terminals, two of which are connected to the power supply through 130 m-long coaxial cables [10], and the other two are terminated in a short circuit [9]. The shorted ends are beneficial for beam extraction, owing to the doubled excitation currents. However, the drawback is that these terminal conditions enhance the kicker impedance [11, 12].

The standard method of suppressing the kicker impedance involves inserting matched resistors at the end of the kicker terminals [13]. However, the scheme makes void the merit of the doubled excitation currents with the shorted ends.

To overcome this difficulty, we suggested inserting diodes with matched resistors (diode unit) at the end of the kicker terminals in front of the thyratron switch, as shown in the right panel of Fig. 1 [14, 15]. This scheme guarantees doubled excitation currents with the shorted ends by preventing the forward current created by the Pulse Forming Line (PFL) from flowing into the matched resistor. Meanwhile, the high-frequency beam-induced current can pass through the diodes and is absorbed into the matched resistors suppressing the kicker impedance. This is because diodes act as a capacitor as well as a rectifier for beam-induced currents when a reverse voltage is applied, creating the insulated depletion layer between the anode and cathode sides, in turn reducing the impedance for high-frequency components.

ISBN: 978-3-95450-253-0 ISSN: 2673-5571 doi:10.18429/JACoW-HB2023-TUC4I1

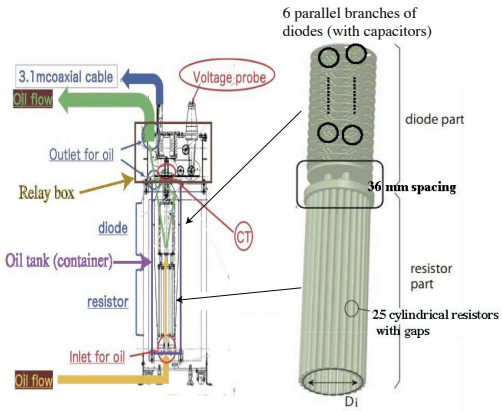

Figure 2: Schematics of a diode unit, installed in an oil tank, which is comprised of 25 cylindrical l_R =455 mm long resistors with d_R = 15 mm diameter cylindrically placed with its diameter D_i =137 mm, 30 parallel 27 series diodes, and 6 parallel and 27 series 1000 pF capacitors.

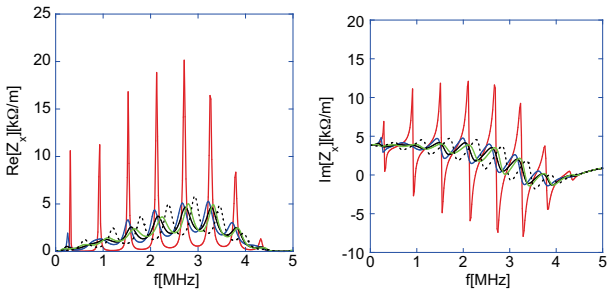

Figure 3: Transverse impedances for β =0.964.

However, additional efforts must be required from a practical point of view, because the heating on diodes and resistors can destroy these parts under the 25 Hz repetition routine operation of RCS. In addition, the fast-rising voltage across diode units during the thyratron switch turning on may cause degradation of the diode stack due to transient voltage. Moreover, the attached diode unit may have a significant effect on the extraction beams from the RCS [16].

STRATEGY TO DESIGN DIODE MODULE

To address these concerns, the diode unit is designed to be cooled by circulating oil, as illustrated in Fig. 2 [17]. To enhance the cooling efficiency, (1) the respective diode modules are in direct contact with the circulating oil, (2) the diode stack makes a ladder structure consisting of 6 parallel branches, supported by insulator bases with slots by which the oil effectively cools the respective diodes, thereby reducing the heat load on them and the synthetic inductance of the diode stack, and (3) capacitors are connected in parallel with the diodes to enhance the durability of the stack, but the synthetic capacity is less than 0.5 nF so that the beams can be stably extracted from the RCS seen in later. In the end, one diode in Fig. 1 consists of 30 parallel and 27 series tiny diodes with l_d length (7.6 mm) and D_d diameter (5.4 mm), and 6 parallel and 27 series 1000 pF capacitors.

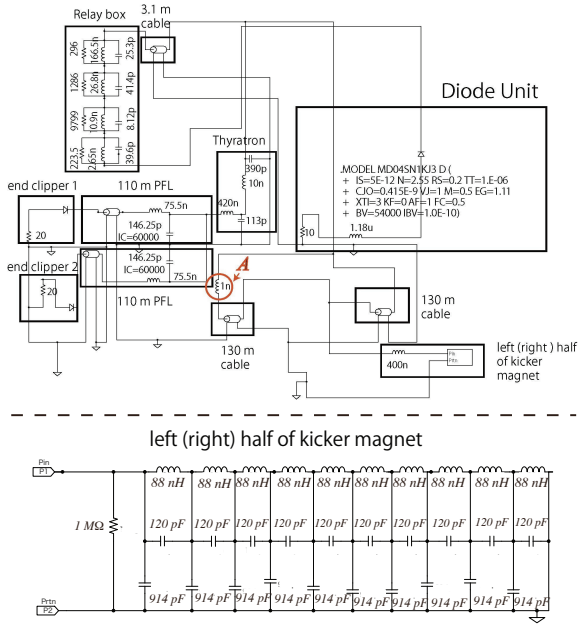

Figure 4: SPICE© simulation model with diode units.

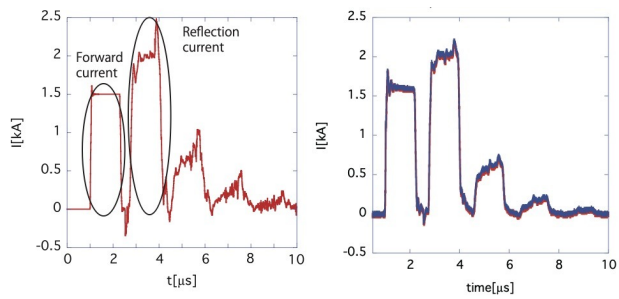

Figure 5: Results with diode unit observed at A in Figs. 1, 4 by simulations (left) and measurements (right).

The voltage probe and current transfer (CT) in Fig. 2 can directly measure the voltage across the diode unit and the current on the unit by which we can observe the coupling impedance with Fourier transformed beam-induced voltage divided by the current as shown in Fig. 3, where the blue, black, and green lines show the results for 240 kW, 480 kW, and 960 kW beams, respectively. The red line shows the theoretical result without a diode unit. The black dotted line shows the hypothetical result, where the thyratron end is terminated by only a 10 Ω resistor. The kicker impedance is drastically reduced, compared to that of the kicker without the diode unit. The parallelized branching of the diode stack makes the impedance almost the same as if only matching resistors were attached to the terminals. The heating rate of the diode units contributed from the beams can be directly measured by the voltage probe and CT to evaluate the durability of the unit, as well.

While reducing the beam-coupling impedance, the kicker must excite the magnetic field to extract beams from the RCS. The SPICE© model for the kicker with diode unit is described in Fig. 4 [17–20], where the location A is identical to that in Fig. 1. The left and right panels in Fig. 5 show SPICE© simulations and measurements observed at

ISBN: 978-3-95450-253-0 ISSN: 2673-5571 doi:10.18429/JACoW-HB2023-TUC4I1

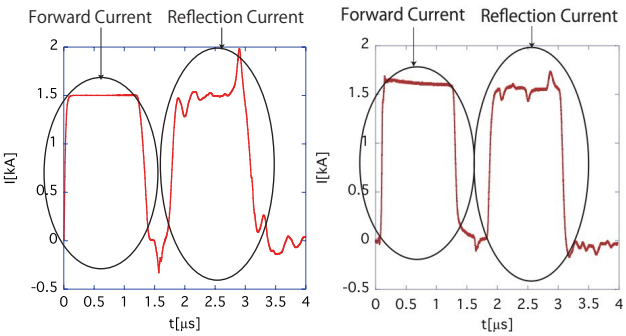

Figure 6: Results without diode unit observed at A in Figs. 1, 4, by simulations (left) and measurements (right).

position A, respectively. For reference, simulations and measurements for the kicker without a diode unit are shown in Fig. 6. The red and blue lines in the right panel of Fig. 5 denote the measured waveforms on the left-hand and right-hand sides of the kicker respectively. The results demonstrate the high reproducibility of the diode unit.

Overall, the simulation matches the measurements. The lingering waveforms with ∼10 μs damping time after the reflection current is created by the impedance mismatch after the attachment of the diode unit to the kicker. Though this may seem to be a drawback, the beam pulse is injected into the RCS 20 ms after the previous beam is extracted. In conclusion, the diode unit causes no problems at the RCS.

The amount of electric power generated in the unit is estimated at about 1.25 kW by measurements and about 1.3 kW by simulations, when no beams contribute, demonstrating the simulation model predicts the heating rate of diode units within 4 % ($\simeq 1 - 1.25/1.3$) accuracy.

The measured 1.25 kW can be divided into the power consumption of the resistors and that of the diodes. The contribution from the resistor is about 1.16 kW based on the fact that the total resistor in the diode unit is 10 Ω, and thus, the contribution from the diode stack is about 0.09 kW. They are used as input parameters to evaluate the heating effect on the unit in the following simulation studies.

Fig. 5 reveals the oscillation on the rising edge of forward currents, which is caused by a 3.1 m-long 20 Ω coaxial cable [10] connecting the diode unit to the thyratron in Fig. 1 [17]. The effect on the extraction beams from the RCS seems significant from a viewpoint of only the observation of waveform currents. Hence, let us directly evaluate it by measuring the trajectory of extraction beams from the RCS.

THE EFFECT OF THE DIODE UNIT ON THE EXTRACTED BEAM

There are in total eight kicker magnets at the extraction section in the RCS. To detect the fluctuations on the flat top kicker fields, we use the fact that the ringing on the flat-top fields displaces the extracted beam horizontally from the ideal trajectory at the downstream beamline of the RCS. In the RCS, there are two kinds of trigger systems for the kicker power supply. One timing module controls the entire trigger timing of the thyratrons for all eight kicker magnets,

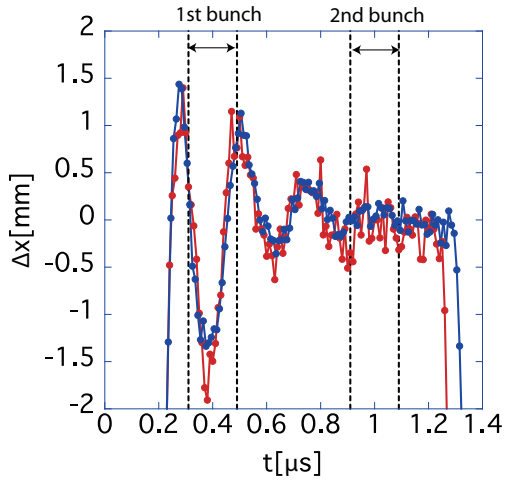

Figure 7: Comparison of the deviation of the extracted beam positions with (red) and without (blue) diode units.

while the other timing module does the individual trigger timing for the respective kicker magnets. The degree of field flatness for one kicker was found via the beam position shift measured by a beam position monitor installed at the downstream beamline of the RCS when the trigger timing for the assigned kicker pulse was changed step by step [21].

Fig. 7 illustrates the 10 times averaged measured trajectory (closed circle), at the down streamline, of the extracted beams with about 30 ns longitudinal full width, where one bunch beam with 8.5×10^{11} particle per bunch is accelerated under full chromaticity correction. The arrival timings and widths of the first and second bunches under the user operation are specified with the dashed lines.

The measured maximum amplitude ranges from approximately 1.5 mm to 2 mm for the case with the diode unit. Even when no diode units are attached, the significant modulation can be identified, which attributes to the structure of the magnet, i.e. the mutual inductance between the coils in the kicker.

At the RCS, the effective flatter trapezoidal field is produced during the extraction time for user operation by adjusting the thyratron timings among eight kickers. A chip appearing at the back of the second bunch in Fig. 7 shortens the flat top time owing to the unit. However, the effect is not a significant drawback when producing an effective flatter trapezoidal field from a practical perspective, as there is still enough margin in the flat top duration. In this sense, the difference between with and without the unit is negligible.

HEATING EFFECT ON THE DIODE UNIT

To put the diode unit into practical use, we need to understand the relationship between its heating rate and the oil flow to design the diode unit to be efficiently cooled by the specified oil flow. Under the present specification, the maximum temperature must be below 150 °C for the resistors [22] and 85 °C for the respective diodes as determined by their terminal conditions [23].

ISBN: 978-3-95450-253-0 ISSN: 2673-5571 doi:10.18429/JACoW-HB2023-TUC4I1

The surface temperature T_R of the respective cylindrical resistors in Fig. 2 can be calculated from Newton's law of cooling as [24],

$$T_R = T_o + \frac{w_R}{h l_R \pi d_R \times 10^{-3}}, \quad (1)$$

where T_o is the temperature of the surrounding oil, and h is the heat transfer coefficient. The heat transfer coefficient is

$$h = \frac{7\lambda}{d_R \times 10^{-3}} = 70 \ [\mathrm{W/m^2 \cdot K}], \quad (2)$$

following the Nusselt number formula proposed by Churchill-Bernstein [25], with the oil flow and the thermal conductivity of oil being 6.5 L/min and $\lambda = 0.15$ W/m·K [26], respectively. The heating rate due to a cylindrical resistor, w_R is calculated as

$$w_R = \frac{1160}{25} = 46.4 \ [\mathrm{W}], \quad (3)$$

when the total heating rate owing to 10 Ω is 1.16 kW. Finally, the surface temperature T_R of the cylindrical resistor can be calculated as follows,

$$T_R = T_o + \frac{w_R}{h l_R \pi d_R \times 10^{-3}} = T_o + 31. \quad (4)$$

The estimation suggests that the surface temperature of the cylindrical resistor could rise by 31 °C relative to the temperature of the surrounding oil. For example, when the temperature of the oil reaches 40 °C, this rough estimation suggests that the surface of the resistor could be 71 °C, which is sufficiently lower than 150 °C.

Similarly, the surface temperature T_d of the cylindrical tiny diode is evaluated as follows,

$$T_d = T_o + \frac{iv}{h l_d \times 10^{-3} \pi D_d \times 10^{-3}} = T_o + 7.75, \quad (5)$$

where the heating rate iv due to one mini-diode is

$$iv = \frac{90}{30 \times 27} = 0.1 \ [\mathrm{W}], \quad (6)$$

and

$$h = \frac{\lambda 3.63}{D_d \times 10^{-3}} \simeq 100 \ [\mathrm{W/m^2 \cdot K}], \quad (7)$$

where we assume that the total heating rate due to the total diode part is 90 W. Hence, if the oil temperature reaches 40 °C, the surface of the mini-diode could be roughly 47.75 °C, which is also sufficiently lower than 85 °C.

Numerical simulation is executed by using ANSYS Fluent© [27]. The structure of the diode unit is similar to that of a Pin Pitch Heat Sink. Hence, the oil flow is analyzed in detail based on the "k-ϵ with RNG model" [28, 29]. This method is employed based on its applicability to cases where the flow becomes turbulent only near a structure and becomes re-laminarized after passing through the structure. Such flow behavior could occur around diodes and resistors including holes and slits, where the flux is changing due to the geometry change.

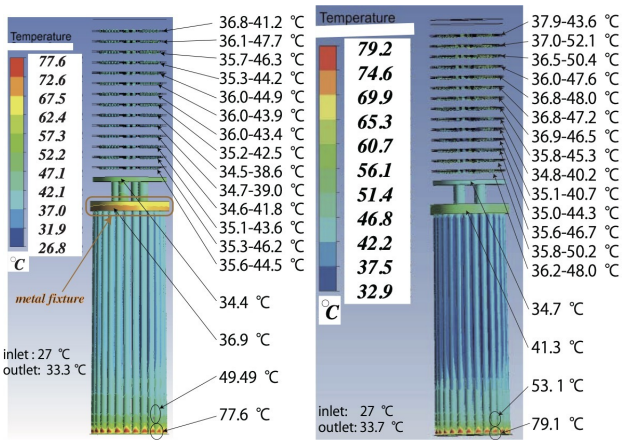

Figure 8: Temperature distribution on the diode unit with radiation effects and without beam heating effects (left) and with both radiation and 1-MW beam heating effects (right).

In the simulation, we impose the heat flux on the surface of the mini-diode and the cylindrical resistor as the thermal condition. The surfaces on the diode, the resistors, and their metal fixtures are in contact with the flowing oil. To account for the heat transfer from the diodes and resistors to these materials (metal and oil), we adopt "coupled" boundary conditions of the diodes and resistors in ANSYS Fluent©. The radiation effect is taken into consideration by setting "Internal Emissivity" to one, assuming the diodes and resistors are black bodies.

Figure 8 shows the simulations obtained without (left) and with beam (right) contributions to the heating. The results without (with) beam contribution reveal that the oil temperature from the outlet is 33.3 (33.7) °C and the one from the inlet is 27 (27) °C, meaning an oil temperature rise $\Delta T^{(c)}$ equal to 6.3 (6.7) °C (refer to Fig. 9).

Without beam contributions (left), the diode temperature ranges from 34.5 °C to 47.7 °C while the temperature of the oil surrounding the diodes can be roughly estimated as ∼ 30 °C. Hence, the difference between the average temperature of the diodes and the temperature of the oil is estimated as $(47.7 + 34.5)/2 - 30 \simeq 11$ °C. This value is somewhat higher than the value analytically estimated from Eq. 5 (7.75 °C), but is still a good rough estimate.

The temperature of the resistor ranges from 36.9 °C to 77.6 °C in the left panel of Fig. 8. The oil flows from the center of the oil tank bottom (the inner side of the resistors) to the outer side of the resistors. Therefore, the highest temperature and lowest parts are at the bottom and top of the resistors, respectively. The difference between the average temperature on the resistor and the surrounding temperature (∼ 30 °C) is calculated as $(77.6 + 36.9)/2 - 30 \simeq 27$ °C. The result is more consistent with the analytical estimate of 31 °C obtained from Eq.(4), thanks to the simpler structure of the resistor part compared with that of the diode part.

Overall, the analytical manner without radiation effects surprisingly provides relatively good estimates for the

ISBN: 978-3-95450-253-0 ISSN: 2673-5571 doi:10.18429/JACoW-HB2023-TUC4I1

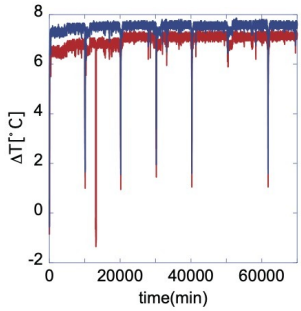

Figure 9: Measurements of $\Delta T(t)$ during 45 days including 830 kW beam contributions.

temperature rise of the resistors and diodes. Therefore, the analytical method can serve as a good guideline for estimating the temperature rise especially at the very early design stage of the diode unit.

Figure 8 reveals the heat conduction on the metal fixing above the resistors; hence, the spacing shown in Fig. 2, with a distance of 36 mm, is effective in suppressing the heat conduction from the resistor part to the diode part.

We also conducted temperature measurements without beam contributions. The prototype kicker power supply was operated for 24 hours to directly measure the surface temperatures of the resistors after attaching the "temperature label" [30] to the lower portion of the resistor part (the site experiencing the highest temperature), as well as the metal plate below the diode part. The measurements demonstrated that no parts are heated beyond 50 °C [17] as shown by simulations in the left panel of Fig. 8.

Finally, the simulations in Fig. 8, including the 1 MW beam contributions, certify that the temperatures at the diodes and resistors terminals are sufficiently lower than 85°C for diodes and 150 °C for resistors.

It is possible to indirectly detect the state of the diode unit by monitoring the oil temperature at the inlet and outlet of the oil tank with thermocouples. Fig. 9 shows the temperature difference $\Delta T(t)$ between at the outlet and the inlet of the oil tank during 45 days of 830 kW beam operation. The red and blue lines represent the results of the diode units for the left-hand and the right-hand sides of the kicker, respectively.

The temperature difference $\Delta T(t)$ saturates to $\Delta T^{(c)}$, which is analytically estimated as follows [17]:

$$\Delta T^{(c)} = \frac{1000W \quad [\mathrm{kW}]}{r\left[\frac{\mathrm{g}}{\mathrm{cm}^3}\right]\frac{1}{60}\mathbb{V}\left[\frac{\mathrm{L}}{\mathrm{min}}\right]4.184\bar{c}_p\left[\frac{\mathrm{cal}}{\mathrm{g\,K}}\right]}, \qquad (8)$$

where W is the heating rate of the diode unit, $\mathbb{V}$ is the oil flow velocity, $r = 0.941$ is the oil specific gravity, and $\bar{c}_p = 382.4$ cal/gK is the oil specific heat [26]. In the case of $\mathbb{V} = 6.5$ L/min and $W = 1.3$ kW under 830 kW beam operation, $\Delta T^{(c)} \simeq 8$ °C, being consistent with the measurements in Fig. 9.

When a 1 MW-beam is accelerated with a repetition rate of 25 Hz, the power consumption of the diode unit is measured to be 61.1 W. This contributes to a temperature rise of the unit, evaluated as $\Delta T^{(c)} \simeq 0.4$ °C, which is negligible

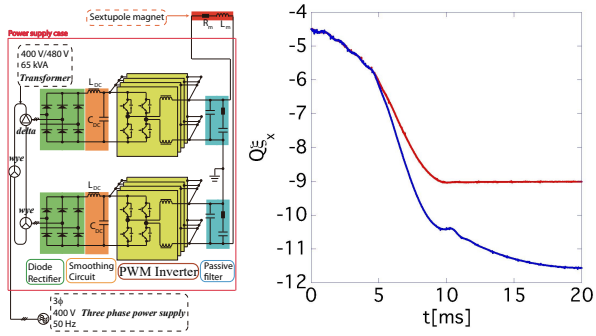

Figure 10: Bipolar power supply for a sextupole magnet (left) [31] and time dependence of the horizontal absolute chromaticity $Q\xi_x$ (right).

compared to a rise of approximately 7.66 °C due to only the PFLs. A comparison of the simulation results shown in the left and right panels of Fig. 8 reveals that the contribution from the beam is $\Delta T^{(c)} = 0.4$ °C, which is consistent with the analytical estimate.

Now, the oil flow and oil temperature can be correlated; therefore, monitoring both the oil temperature and oil flow is a practical way to double-check the unit's malfunctioning.

THE SUPPRESSION OF BEAM INSTABILITY

Finally, we demonstrate the effect of an impedance reduction by the diode unit on the suppression of beam instabilities. Up to now, the diode unit is only attached to "one RCS kicker"among eight kickers installed at the RCS.

In the RCS, the bipolar sextupole magnetic fields have been dynamically manipulating the chromaticity since the fall of 2016 to suppress the beam instability [32–34]. The left panel of Fig. 10 illustrates the configuration of the bipolar power supply, which is comprised of a diode rectifier, a smoothing circuit, a Pulse Width Modulation (PWM) inverter, and a passive filter. The PWM inverter is a voltage-fed H-bridge inverter, whose switching element uses an IGBT of 1400 V-600 A, and the switching frequency is 20 kHz [31].

The right panel of Fig. 10 shows the horizontal absolute chromaticity, where the natural chromaticity is -9 at RCS. The blue line activates the sextupole magnets yield targeting a 1.15 times increase of the chromaticity to suppress the beam instability, while the red line makes the sextupole magnets are gradually turned off so that the chromaticity becomes the natural chromaticity after 10 ms to excite the beam instability.

Figure 11 shows the overlaid results of each of three consecutive measurements (red, blue, and black) at the transverse beam position (number of particles per pulse: 8.1×10^{13} each, unaveraged). The left and the right panels show the results without and with diode units, respectively. The large peak around 0.5 ms does not describe beam instability, because the monitored beam centroids do not precisely express the beam behavior during the first 0.5 ms

ISBN: 978-3-95450-253-0 ISSN: 2673-5571 doi:10.18429/JACoW-HB2023-TUC4I1

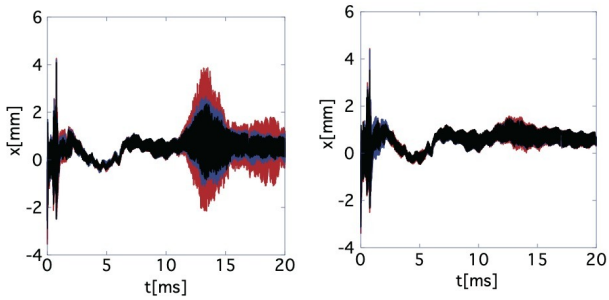

Figure 11: Comparison of measured beam behavior before (left) and after (right) the attachment of the diode unit.

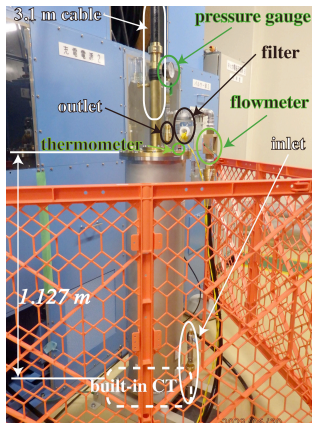

Figure 12: Downsized diode unit, used under the routine operation of RCS (compare to Fig. 2).

since the LINAC beams are injected and accumulated in the RCS while transverse painting is performed in the process. The horizontal beam instability starts around 11 ms during 20 ms acceleration in the left panel. A comparison between the left and right results leads that the beam growth rate is significantly suppressed even after the attachment of the diode units to only one kicker in the RCS.

Note that the suppression of beam instability is realized in the case of the kicker with the diode unit when the unnormalized horizontal and vertical rms emittance at the 3 GeV extraction energy were 6.42π mm.mrad and 5.52π mm.mrad, respectively, measured after 5 successive shots before being averaged [35]. The results are in good agreement with numerical simulation results [17, 36] within factor 1.5. This achievement is remarkable to deliver higher intensity beams with smaller emittance to the MR.

Currently, 6.45×10^{13} particles per pulse, with horizontal and vertical rms unnormalized emittances of 4.5π mm.mrad and 4.2π mm.mrad respectively, at extraction energy, are routinely delivered to the MR in its fast extraction mode for neutrino experiments. As in Fig. 12, the diode unit has been downsized for ease of weekly maintenance, and the CT has been relocated from the top to the bottom of the diode unit (see Fig. 2). The flowmeter and thermometer measurements are employed in the machine protection system, with the pressure gauge corroborating the flowmeter measurements, while the filter prevents accidentally broken tiny diodes from entering the oil circulation system.

CONCLUSIONS

The kicker impedance can be reduced by inserting diodes and resistors at the switch end of the coaxial cables. This scheme ensures doubled excitation currents for the extraction beam by inverting the voltage wavefront and superposing the excitation currents with two shorted ends, which is beneficial for power saving. While the resistors are isolated from the switch cathode, they can be seen by high-intensity beam-induced currents, thereby reducing the kicker impedance.

We have designed a diode stack with a ladder structure to increase the parallel branches of the diodes. This structure enhances the cooling efficiency of the diode unit by the oil, reducing the synthetic inductance of the diode stack and the heating load on the stack. In the end, the kicker impedance is at a comparable level to that of the case with only a matched resistor attached to the kicker.

Analytical estimates of the diodes and resistors surface temperature are in agreement with simulations conducted with ANSYS Fluent©. From a practical standpoint, the analytical estimation of the temperature increase in the diode unit can serve as a valuable guideline for designing the diode unit, particularly in its initial stages.

The relationship between oil flow and oil temperature increase is analytically established and supported by measurements. Currently, those two values serve as indicators for machine protection at the RCS. Furthermore, the diode stack durability has been demonstrated through a 45-day 830 kW beam user operation.

The current ripple caused by the diode unit during the rising time of the current waveform has a minor effect on the extraction beam. This is because the coupling effects due to mutual inductances between two coils in the kicker could have a more dominant influence on the excited magnetic field than the current ripple caused by the diode unit.

The beams extracted from the RCS are delivered to the MR through the beam extraction line with a small mechanical aperture, resulting in the generation of a large residual dose in the area. To address this issue, it is preferable to create beams with a smaller emittance. As a solution, we accelerated a beam containing 8.3×10^{13} particles per pulse (1 MW-eq), with horizontal and vertical rms unnormalized emittances of $6.42\,\pi$ mm.mrad and 5.52π mm.mrad, respectively, at the extraction energy.

The impedance reduction achieved by the diode unit, even though it is attached to only one of the eight kickers in the RCS, has successfully suppressed beam instabilities [17]. This accomplishment is of great significance for extending the parameter windows in the tune diagram of the RCS to support future higher-power operations of the MR. This is especially critical because the beam growth rate in the beam instability for smaller emittance beams is more pronounced in the space charge-dominated beam, such as in the RCS, due to the mitigation of the suppression effect caused by indirect space charge forces. We have already demonstrated the emittance dependence of the beam growth rate through both theoretical and measurement approaches [7].

ISBN: 978-3-95450-253-0 ISSN: 2673-5571 doi:10.18429/JACoW-HB2023-TUC4I1

REFERENCES

[1] K. Yamamoto *et al.*, "Design and actual performance of J-PARC 3 GeV rapid cycling synchrotron for high-intensity operation", *J. Nucl. Sci. Technol.*, vol. 59, no. 9, 2022 doi:10.1080/00223131.2022.2038301.

[2] J-PARC Annual Report 2014, p. 9, j-parc.jp/documents/annual_report/a_report_2014.pdf

[3] J-PARC website, http://j-parc.jp/index-e.html

[4] A.W. Chao, *Physics of collective beam instabilities in high energy accelerators*, Wiley, New York, 1993.

[5] Y.H. Chin, J. Kamiya, Y. Shobuda, K. Takata, and T. Toyama, "Impedance and Beam Instability Issues at J-PARC Rings", in *Proc. HB'08*, Nashville, TN, USA, Aug. 2008, paper WGA01, pp. 40–44.

[6] Y. Shobuda, P. K. Saha, M. Yamamoto, Y. H. Chin, Y. Irie, and T. Toyama, "The Kicker Impedance and its Effect on the RCS in J-PARC", in *Proc. HB'14*, East Lansing, MI, USA, Nov. 2014, paper THO2AB02, pp. 369–373.

[7] Y. Shobuda *et al.*, "Theoretical elucidation of space-charge effects on the coupled-bunch instability at the 3 GeV rapid cycling synchrotron at the Japan Proton Accelerator Research Complex", *Prog. Theor. Exp. Phys.*, vol. 2017, no. 1, p. 013G01, 2017. doi:10.1093/ptep/ptw169.

[8] P. K. Saha *et al.*, "Simulation, measurement, and mitigation of beam instability caused by the kicker impedance in the 3-GeV rapid cycling synchrotron at J-PARC", *Phys. Rev. Accel. Beams*, vol. 21, p. 024203, 2018. doi:10.1103/PhysRevAccelBeams.21.024203.

[9] J. Kamiya, T. Takayanagi, and M. Watanabe, "Performance of extraction kicker magnet in a rapid cycling synchrotron", *Phys. Rev. Spec. Top. Accel. Beams*, vol. 12, p. 072401, 2009. doi:10.1103/PhysRevSTAB.12.072401.

[10] Fujikura Ltd. website, https://www.fujikura.com/

[11] Y. Shobuda, Y. Irie, T. Toyama, J. Kamiya, and M. Watanabe, "Measurement scheme of kicker impedances via beam-induced voltages of coaxial cables", *Nucl. Instrum. Methods Phys. Res., Sect. A*, vol. 713, no. 52, 2013. doi:10.1016/j.nima.2013.02.037

[12] Y. Shobuda, Y. Irie, and T. Toyama, "Analytical approach to evaluate coupling impedances of traveling kicker magnets", textitNucl. Instrum. Methods Phys. Res., Sect. A, vol. 691, no. 135, 2012. doi:10.1016/j.nima.2012.06.066

[13] W. Zhang *et al.*, "SNS Extraction Fast Kicker Pulsed Power System", in *Proc. EPAC'04*, Lucerne, Switzerland, Jul. 2004, paper WEPKF087, pp. 1810–1812.

[14] Y. Shobuda, *et al.*, "Reducing the beam impedance of the kicker at the 3-GeV rapid cycling synchrotron of J-PARC", *Phys. Rev. Accel. Beams*, vol. 21, p. 061003, 2018. doi:10.1103/PhysRevAccelBeams.21.061003

[15] Y. Shobuda, Y. Irie, T. Takayanagi, T. Togashi1, K. Yamamoto, and M. Yamamoto, "Reduction of the kicker impedance maintaining the performance of present kicker magnet at RCS in J-PARC", *J. Phys. Conf. Ser.*, vol. 1067, no. 6, p. 062007, 2018. doi:10.1088/1742-6596/1067/6/062007

[16] E. Koukovini-Platia, M.J. Barnes, H. Bartosik, G. Rumolo, L. Sermeus, and C. Zannini, "Source of horizontal instability at the CERN Proton Synchrotron Booster", *Phys. Rev. Accel. Beams*, vol. 22, p. 124201, 2019. doi:10.1103/PhysRevAccelBeams.22.124201.

[17] Y. Shobuda *et al.*, "Demonstration of a kicker impedance reduction scheme with diode stack and resistors by operating the 3 GeV rapid cycling synchrotron of J-PARC", *Phys. Rev. Accel. Beams*, vol. 26, p. 053501, 2023. doi:10.1103/PhysRevAccelBeams.26.053501

[18] M. Watanabe *et al.*, "Operation and current status of injection, extraction, kicker magnet and the power supply for J-PARC 3 GeV RCS", in *Proc. IPAC'12*, New Orleans, LA, USA, May 2012, paper THPPD052, pp. 3629–3631.

[19] SPICE©(Simulation Program with Integrated Circuit Emphasis), https://en.wikipedia.org/wiki/SPICE

[20] TopSpice©, https://penzar.com/topspice/topspice.htm

[21] H. Harada *et al.*, "Beam-based compensation of extracted-beam displacement caused by field ringing of pulsed kicker magnets in the 3 GeV rapid cycling synchrotron of J-PARC", *Prog. Theor. Exp. Phys.*, vol. 2017, p. 093G01, 2017. doi:10.1093/ptep/ptx125

[22] Tokai konetsu kogyo Co., Ltd, https://www.tokaikonetsu.co.jp/english/product/as-and-ash/

[23] Origin Company Limited website, https://www.origin.co.jp/eng/

[24] F. P. Incropera, D. P. Dewitt, T. L. Bergman, and A. S. Lavine, *Fundamentals of heat and mass transfer*, 6th Ed., New York, NY, USA: John Wiley & Sons, 2006.

[25] S. W. Churchil and M. Bernstein, "A correlating equation for forced convection from gases and liquids to a circular cylinder in crossflow", *J. Heat Transfer*, vol. 99, 1977. doi:10.1115/1.3450685

[26] Shin-Etsu, "Silicone fluid performance test results", http://www.shinetsusilicone-global.com/catalog/pdf/kf96_e.pdf

[27] ANSYS Fluent©, https://www.ansys.com/products/fluids/ansys-fluent

[28] ANSYS© 4.4.2 RNG k-ϵ model, https://www.afs.enea.it/project/neptunius/docs/fluent/html/th/node59.htm

[29] S. A. Orszag, *et al.*, "Renormalization group modeling and turbulence simulations", in *Proc. Int. Conf. Near-Wall Turbulent Flows*, Tempe, Arizona, Mar. 1993, p. 1031

[30] NiGK Corporation Temperature Label datasheet, www.nichigi.co.jp/en/en_downloadform/en_data.html

[31] Y. Watanabe, T. Adachi, S. Igarashi, H. Someya, and N. Tani, "Rapid-cycling power supplies for the J-PARC RCS sextupole magnets", in *Proc. IPAC'11*, San Sebastian, Spain, Sep. 2011, paper THPO003, pp. 3338–3340.

[32] Y. Shobuda *et al.*, "Coupled bunch instability and its cure at J-PARC RCS", in *Proc. IPAC'17*, Copenhagen, Denmark, May 2017, pp. 2946–2949. doi:10.18429/JACoW-IPAC2017-WEPIK014

ISBN: 978-3-95450-253-0 ISSN: 2673-5571 doi:10.18429/JACoW-HB2023-TUC4I1

[33] H. Hotchi *et al.*, "Realizing a high-intensity low-emittance beam in the J-PARC 3 GeV RCS", in *Proc. IPAC'17*, Copenhagen, Denmark, May 2017, pp. 2470–2473. doi:10.18429/JACoW-IPAC2017-WEOAA3

[34] P. K. Saha *et al.*, "Dynamic variation of chromaticity for beam instability mitigation in the 3-GeV RCS of J-PARC", in *Proc. IPAC'19*, Melbourne, Australia, May 2019, pp. 171–173. doi:10.18429/JACoW-IPAC2019-MOPGW037

[35] S. Meigo *et al.*, "Beam commissioning for neutron and muon facility at J-PARC", *Nucl. Instrum. Methods Phys. Res., Sect. A*, vol. 600, 2009, pp. 41–43 doi:10.1016/j.nima.2008.11.068

[36] H. Hotchi, "Effects of the Montague resonance on the formation of the beam distribution during multiturn injection painting in a high-intensity proton ring", *Phys. Rev. Spec. Top. Accel. Beams*, vol. 23, p. 050401, 2020. doi:10.1103/PhysRevAccelBeams.23.050401